over the north sea," *J. Geophys. Res.*, vol. 92, pp. 13 127–13 139, 1987.
[9] S. D. Smith, "Coefficients for sea surface wind stress, heat flux, and wind profiles as a function of wind speed and temperature," *J. Geophys. Res.*, vol. 93, pp. 15 467–15 472, 1988.

A Coherent Dual-Polarized Radar For Studying the Ocean Environment

Simon Haykin, C. Krasnor, T. J. Nohara, Brian W. Currie, and D. Hamburger

Abstract—**The important features of a coherent dual-polarized *X*-band radar, designed to be of instrumentation-quality for research use, are described. The motivation for building the radar is to quantify the improvements attainable through the use of (a) coherence, and (b) polarization in the detection of small floating targets in the presence of sea clutter. Results on the statistics of dual-polarized radar returns from the ocean surface (obtained with this radar at a site on the east coast of Canada) are presented. These results indicate that the *K*-distribution is very useful for describing the amplitude statistics of sea clutter (both the like- and cross-polarized channels) for low grazing angles. Analysis of the time-varying Doppler spectra of a small ice target and the neighboring sea clutter reveals differing Doppler characteristics, offering improved target detection.**

I. Introduction

Ordinarily, commercially available marine radars rely solely on amplitude as the radar discriminant, with the result that they are of limited practical use in the detection of small surface targets in the presence of sea clutter. It was the recognition of this fact that prompted the Communications Research Laboratory (CRL) of McMaster University to undertake the design and development of a multi-dimensional radar for ocean surveillance [1].

The radar is known as the IPIX radar [2]. It is a coherent dual-polarized *X*-band radar, designed to be of instrumentation-quality for research use. The radar was built as part of the larger research effort with the aim of developing improved techniques for the detection and identification of small targets in an ocean environment by developing algorithms to utilize the available radar features, and quantify the performance improvement afforded by each. The foundation for this research study must be a thorough understanding of the nature of the sea clutter and the corresponding behavior of targets of interest under various sea conditions. To this end, the IPIX radar is being used to build a data base of sea clutter and target radar returns to characterize the ocean environment and target behavior with respect to the available radar parameters. This communication presents results related to some studies of improvements attainable through the use of (a) coherence, and (b) polarization in the detection of small floating (surface) targets in the presence of sea clutter.

Manuscript received October 20, 1989; revised March 21, 1990. This work was supported in part by Litton Systems Canada Ltd., in part by the Natural Sciences and Engineering Research Council of Canada, and in part by the Ontario Ministry of Colleges and Universities.

The authors are with the Communications Research Laboratory, McMaster University, 1280 Main Street West, Hamilton, ON L8S 4K1, Canada.

IEEE Log Number 9040631.

II. IPIX Radar Features

Development of the IPIX radar began in 1984, and a prototype was tested in the summer of 1986. The IPIX radar has the following features [2]:

1) 8-kw pulsed transmitter using a TWT amplifier operating at 9.39 GHz;
2) coherence, to permit Doppler processing;
3) dual linear polarization with pulse-to-pulse transmit polarization switching so as to acquire the full polarization scattering matrix;
4) a surface acoustic wave (SAW) pulse compression subsystem, providing improved resolution and range of coverage (a 5-μs transmitted expanded pulse is compressed to an effective pulsewidth of 32 ns in the receiver, equivalent to a range resolution of 4.8 m and a transmitted peak power of 1.2 MW);
5) computer control, for highly flexible control of radar parameters and data acquisition (computer involvement includes antenna position control, pulse repetition frequency (PRF) and pulsewidth selection, downloadable sensitivity time control (STC) curves, windowing of data collection area in range and azimuth, and transmit polarization selection, among others);
6) digital data acquisition with in-field processing capability to facilitate algorithm development efforts and provide on-site data validation (four channels of 8-b digital data are collected: vertical and horizontal polarization, each with in-phase and quadrature signals);
7) built-in calibration equipment allowing automated in-field system calibration.

The IPIX radar is specifically designed to be a research instrument. Digital control allows experimental parameters to be easily varied, but once selected they remain accurate and stable. Built-in calibration equipment permits quantitative measurements to be made with high confidence. The data acquisition system delivers digital radar data at real-time rates into the address space of a computer, where it may be validated, processed, and stored on removable media for off-line analysis. The computer control system facilitates precise experiment documentation, describing the complete state of the radar system, which is stored with the collected data.

Future expansion of the IPIX radar includes the provision of a simultaneous dual-frequency capability to measure the space/time coherence of a target [3]. The space/time coherence is a measure of the rigidity of the target. This technique, therefore, holds the promise of distinguishing floating solid objects from the fluid ocean surface—a major objective of marine radar. Current marine radars, however, cannot reliably detect a solid object if its protrusion above the surface is similar in height to the surrounding waves.

III. Statistics of Dual-Polarized Return Amplitudes

This section investigates the use of the *K*-distribution to describe the amplitude statistics of the dual-polarized radar returns and to determine possible improvements in target detection using the cross-polarized channel. The analysis is based on data collected during experiments conducted with the IPIX radar at a coastal site at Cape Bonavista, Newfoundland, in May/June 1989. The radar antenna was 22 m above sea level, a height typical of that of a ship-mounted antenna, and representing a low grazing angle situation.

The *K*-distribution [4] is based on an underlying physical model that treats the received signal as a superposition of returns from a number of independent patches or scatterers, illuminated by the radar beam. The effective number of scatterers is critical in determining the overall statistics of the received data. Measurements

0196-2892/91/0100-0189$01.00 © 1991 IEEE

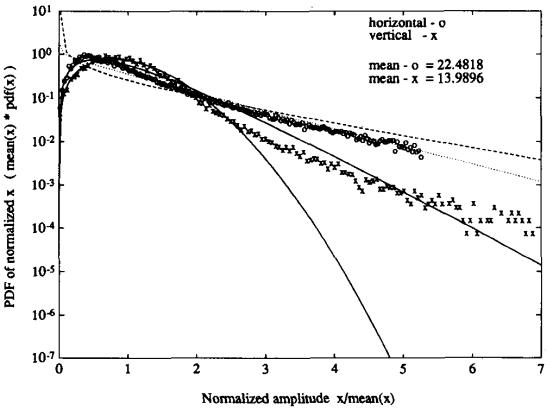

Fig. 1. Normalized amplitude distribution of sea clutter in front of ice target, for pulsewidth of 200 ns and horizontal transmitter polarization. Experimental data for like-polarized horizontal (*HH*) channel is indicated by (○), and cross-polarized vertical (*HV*) channel by (×). *K*-distribution curves fitting data are shown, with shape parameter $v = 0.45$ for *HH*, and $v = 1.7$ for *HV*. Also shown are limiting cases for *K*-distribution: lowest curve representing Rayleigh distribution (v = infinity), and top curve ($v = 0.25$) approaching lognormal.

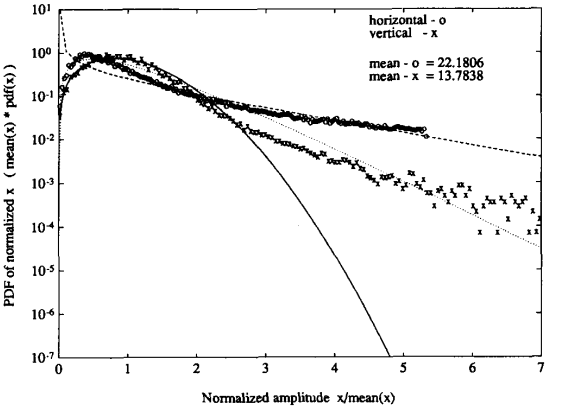

Fig. 2. Normalized amplitude distribution of ice target in sea clutter, for pulsewidth of 200 ns and horizontal transmitter polarization. Experimental data for like-polarized horizontal (*HH*) channel is indicated by (○), and cross-polarized vertical (*HV*) channel by (×). *K*-distribution curves fitting data are shown, with shape parameter $v = 0.25$ for *HH*, and $v = 1.4$ for *HV*. Also shown is limiting case for *K*-distribution for large v: lowest curve representing Rayleigh distribution (v = infinity).

were taken for a variety of pulsewidths and polarizations with the antenna stationary. The amplitude data were calculated as the magnitude of the *I*-*Q* samples.

Figs. 1 and 2 show examples of the statistical analysis. In the figures, the normalized amplitude histogram of the data is plotted on a log scale. The data received by the horizontally polarized channel are marked with an ○ and the data received by the vertically polarized channel are marked with an ×. Along with the data curves, some pertinent *K*-distribution curves are also plotted. The solid line indicates the Rayleigh curve and the dashed line corresponds to $v = 0.25$. Furthermore, appropriate *K*-curves are also drawn through the measured data points, and their shape parameter v is indicated at the top of each figure.

Figs. 1 and 2 are based on a set of measurements taken using a 200-ns pulse to sample a small ice target, using a horizontal transmit polarization (*HH* and *HV* collected). The target was located at a range of 6.0 km and bearing of 116°. The winds were from the northeast at under 10 kn. From photography, the ice target was estimated to be a small bergy bit or large growler, about 2 m high (above the water) and about 10 m across. Fig. 1 corresponds to sea clutter measurements made in front of and nearby this growler. Fig. 1 indicates that the *K*-distribution is very useful for describing the statistics of sea clutter (both the like- and cross-polarized channels) for low grazing angles using the IPIX radar. In all cases examined, including other pulsewidths and transmitted polarizations, the like-polarized measurements fit the *K*-distribution very closely. Although the cross-polarized measurements do not agree with the *K*-curves as closely, the range of measurements in the cross channel is consistent with the *K* distribution.

Fig. 2 corresponds to measurements made from the growler itself. In spiky clutter such as this, using merely an amplitude threshold will either introduce high false-alarm rates or, alternatively, desensitize the detector. This problem is evident for the growler, where virtually no difference exists in the mean amplitude level of the growler plus sea clutter and that of its surroundings. Furthermore, these results indicate that using the cross-polarized channel for small ice target detection has no apparent advantage. That is, the growler does not appear to stand out from its surroundings any more in the cross channel than it does in the like channel, at least when using only long-term amplitude statistics for each channel.

IV. Time-Varying Spectra of Coherent Radar Returns

This section presents some preliminary results of examining the time-varying Doppler spectra of an ice target in a sea clutter background. The differences in the time-frequency characteristics of the ice target and the sea clutter permit their separate identification, leading to improved target detection.

The same ice target as in the previous section was sampled at a range of 6.5 km at bearing 115°. The ocean had a significant wave height of 1.6 m, and a period of 11 s, as measured by a nondirectional waverider. Both the growler and the waves were approaching the radar at an oblique angle. The winds were light. The data set was collected with the antenna stationary. The radar pulse width was 200 ns, and the transmitter polarization was horizontal (*H*). The range sampling window was reduced to 40 samples, representing a distance of 200 m. This window and the size of the sampling buffer permitted collection of 68 608 successive sweeps at a 2000-Hz PRF, representing a time dwell of just over 34 s.

From the data set, two range positions within the sampling window were selected: one for the growler plus sea clutter and one for sea clutter only. For each range position, data were extracted to yield the *I*-*Q* samples for the 68 608 successive sweeps. These time series were divided into 134 successive blocks of 512 complex samples, for input to a fast Fourier transform (FFT) routine. The resulting magnitude of the FFT was scaled for display by mapping onto the 0–225 grey scale. Fig. 3(a) shows the resulting FFT magnitude display for the *HH* (upper) and *HV* (lower) channels for the growler plus clutter. Each line shows the magnitude of a single 512-point Doppler spectrum (zero Doppler frequency in the middle), with the 134 successive lines (spectra) representing just over 34 s of time. The spectra for each channel are all normalized by the same value. However, the normalization for the cross-polarized channel was a factor of 20 less than the like-polarized channel. This was done to allow the weaker cross-polarized returns to be visible. Three major observations may be made from Fig. 3(a). First, the Doppler return from the growler is clearly visible as the "wiggling" white line. This growler spectral peak is apparent on both the like- and cross-polarized channels. Second, the white areas near and to the right of the growler line are due to sea clutter. Third, the dark bands within the time history of the spectra show areas of no significant return, that is, primarily noise. The period

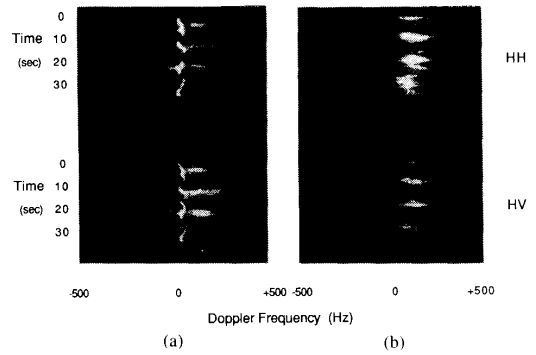

Fig. 3. (a) Display of time-varying Doppler spectra for ice target in sea clutter. Upper part of image is for like-polarized (*HH*) channel, and lower part is for cross-polarized (*HV*) channel. Wiggly line is Doppler peak due to ice target, while more diffuse area to right is due to sea clutter. Intervening dark bands are due to return signal reduction as result of wave obscuration of resolution cell contents by sea swell. Note that weaker cross-polarized spectra have been normalized with value 20 times smaller than that used for like-polarized spectra. (b) Display of time-varying Doppler spectra for sea clutter only, but taken from same data set as for Fig. 3(a). Upper part of image is for like-polarized (*HH*) channel, and lower part is for cross-polarized (*HV*) channel. Again, sea clutter has diffuse spectra. Intervening dark bands are due to return signal reduction as result of wave obscuration of resolution cell contents by sea swell. *HH* spectra have been normalized with value ten times smaller than that of *HH* in (a), while *HV* spectra are normalized with same value as for *HV* in (a).

of these three cycles of noise within the 34 s of data relates directly to the 11 s period of the ocean waves. The ocean swell is causing periodic wave obscuration of the contents (both ice and sea) of the range cell, yielding a noise-only return. Fig. 3(b) shows a similar display for sea clutter only, again with different like- and cross-polarized normalizations to improve visibility. The effect of the swell is obvious here as well.

Examination of Fig. 3(a) and (b) reveals that the more narrow nature of the growler spectral peak (related to its higher spatial coherence), as compared to the more diffuse spectrum of the sea clutter, shows Doppler processing to hold considerable promise for the improved detection of small floating targets in a sea clutter background. The CRL is currently researching suitable processing algorithms to take advantage of these differing Doppler characteristics.

V. Conclusion

This communication has presented results of investigations into the use of dual-polarization and coherence for the improved detection of small targets in an ocean environment. Regarding dual polarization, the *K*-distribution was used to describe the amplitude statistics of both the like- and cross-polarized channels. It was concluded that the cross-polarized channel offered no improvement in target detectability. Regarding coherence, the nature of the time-varying Doppler spectra for an ice target as compared to the neighboring sea clutter showed a significant difference, indicating improved target detection possibilities. Research into signal processing algorithm development and the quantization of detection improvement gains is now being conducted. This study will also include the use of additional radar parameters and features, such as multifrequency transmission.

References

[1] S. Haykin, B. W. Currie, E. O. Lewis, and K. A. Nickerson, "Surface-based radar imaging of sea ice," *Proc. IEEE*, vol. 73, no. 2, pp. 233-251, 1985.

[2] C. Krasnor, S. Haykin, B. W. Currie, and T. Nohara, "A coherent dual-polarized radar for ice-surveillance studies," presented at the Int. Radar Conf., Paris, France, Apr. 1989.

[3] D. T. Gjessing, *Target Adaptive Matched Illumination Radar: Principles and Applications*. London: Peter Peregrinus, 1986.

[4] E. Jakeman and P. N. Pusey, "A model for non-Rayleigh sea echo," *IEEE Trans. Antennas Propagat.*, vol. AP-24, no. 6, 1976.

On Intercommunication Between Microwave and Infrared Radiation Fields and the Condition of Natural Objects

Eugenij A. Reutov

***Abstract*—The energy balance equation of the agricultural geosystem has been considered. The feasibility of remote sensing for estimating the parts of this equation is shown. The intercommunication of microwave and infrared radiation fields, meteorological information about air temperature dynamics, and the total condition of natural objects is considered. It is shown that for the estimation of the total condition of an agricultural geosystem, the absolute measurements of brightness temperatures at microwave and infrared ranges are not required.**

I. Introduction

The management of natural objects over large areas (primarily in agriculture) needs near-real-time and reliable information about its condition. Clearly, remote sensors are necessary to obtain this information over large areas.

This problem may be addressed in two ways. The first is the usual one that relies on the determination of separate soil and canopy parameters (N) such as moisture, temperature, salinity, biomass, etc., using remote sensors. Generally, potential users of remotely sensed data (e.g., in agriculture) using these separate parameters will estimate the total condition of natural objects to make a technical decision. This approach is represented in Fig. 1(a). The realization of the scheme in this figure is very complex and not very reliable because it requires (i) multichannel remotely sensed data ($I_1 \cdots I_i$) according to the number N_i of measured natural object parameters, (ii) adequate physical or statistical models such as

$$\begin{aligned} I_1 &= F_1(N_1 \cdots N_i) \\ I_n &= F_n(N_1 \cdots N_i) \end{aligned} \tag{1}$$

(iii) the solution of system of equations like (1) to determine the N_i parameters, and (iv) models for estimation of the total condition C using N_i values. Each problem listed is quite complex and not always soluble.

The second approach is to delineate the condition C of these objects using the parameters I_i that could be directly measured with remote sensors (for example, the brightness temperature at micro-

Manuscript received November 10, 1989; revised February 21, 1990.

The author is with the Institute of Radio Engineering and Electronics, USSR Academy of Sciences, Karl Marx Avenue 18, GSP-3, Moscow 103907, USSR.

IEEE Log Number 9035827.